Saturated Absorption Spectroscopy of Rubidium Isotopes

Samuel Bellenchia* and Cormac Killeen†
Stony Brook University
Department of Physics and Astronomy
(Dated: April 29, 2019)

In this experiment, we use a diode laser– a semiconductor device which creates a laser beam at the diode junction– to resolve the absorption spectrum of the two naturally occurring forms of Rubidium; ^{85}Rb and ^{87}Rb.To measure the frequency of fine-structured transitions we employ methods of Doppler-Free spectroscopy, which resolve the frequencies typically obscured by the Doppler effect that arise from the randomly distributed velocities of atoms in a particulate gas.

I. INTRODUCTION

Albert Einstein's 1917 paper "The Quantum Theory of Radiation" laid the groundwork for all modern laser technology [3]. His description of stimulated emission and absorption violated our prior understanding of the interaction between matter and radiation.[1][2]

Our experiment relies heavily on the theory of Stimulated Emission and Absorption. Let us assume the simplest model and then elaborate given our specific constraints. Consider an atom with one electron that can occupy two states, ψ_1 and ψ_2, each with respective energies E_1 and E_2. Their *transition energy* is described by $\Delta E = \hbar\nu$ where ν is the frequency of a photon which can either be emitted or absorbed depending on the transition.

Note that in practice one does not observe such exact measurements of absorption as a function of frequency, especially at room temperature. In an atomic gas, atoms are endowed with kinetic energy and therefore velocity, which when relative to the propagation of our light beam incites a Doppler-Effect. This causes our absorption spectrum to "broaden" by following a Maxwell-Boltzmann distribution, which is explained in the following section. [4]

These spacious Gaussian curves where our sharp spectral lines should be is exactly the reason we've created more sophisticated spectroscopy techniques. In Rubidium, the "splitting" of energy states result in absorption peaks that are otherwise obscured by Doppler broadening. The purpose of this experiment is to find the Doppler-broadened peaks corresponding to atomic transitions, then perform "Doppler-Free," or Saturated spectroscopy in hopes to uncover the fine and hyper-fine structure energy levels of our absorption spectrum.

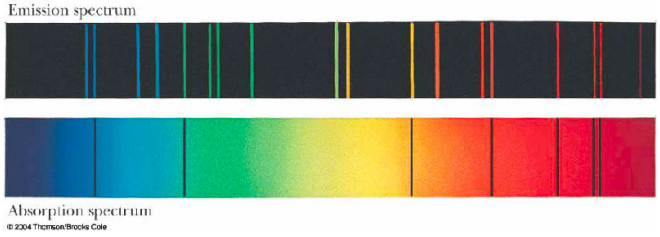

FIG. 1. A visual interpretation of specific light frequencies being absorbed/emitted by an atom. Note, Rubidium's excitation energies lie outside the visible-light spectrum. [13]

A. Unsaturated Spectroscopy

Temperature of a gas is closely related to the Kinetic energy of the moving particles within it, and thus their velocities. The movement of particles in an ideal gas follow a "Maxwell-Boltzmann distribution." Consider an atomic vapor at temperature T of , each with mass m. We are interested in the distribution of velocities component's along the direction of our laser beam's propagation, v_b. The *probability* of a Rubidium atom having velocity between v_b and $v_b + dv_b$ is:

$$n(v_b)dv_b = \sqrt{\frac{m}{2\pi k_B T}} e^{-\frac{mv_b^2}{2k_B T}} dv \tag{1}$$

Now, since the particles are not at rest, the typical absorption frequency will differ based on the Doppler Effect.

The non-relativistic Doppler Effect tells us the absorption frequency in the lab's frame of reference –for an atom with a resting absorption frequency of ν_0 –will be:

$$\nu_{\text{experimental}} = \nu_0(1 \pm \frac{v_b}{c}) \tag{2}$$

We know for light in a vaccuum, $c = \lambda\nu$ where λ is the light's wavelength. Thus, $dv_b = \frac{c}{\nu(V=0)} d\nu_{\text{experimental}}$. We recognize that $\nu(v = 0)$ is simply the resting absorption frequency ν_0. By integrating and substituting the result into equation (1) yields the following;

$$P(\nu_b) = \frac{2}{\delta\sqrt{\pi}} * e^{-\frac{4(\nu_b - \nu_0)^2}{\delta^2}} \tag{3}$$

* bellenchia@gmail.com
† cormac.killeen@stonybrook.edu

Where $\delta = \frac{2\nu_0}{c}\sqrt{\frac{2k_bT}{m}}$ is a function of frequency.

Since equation (3) tells us we have a Gaussian probability density, we can say that the *width* of the gaussian at *half* it's maximum value is $2\delta\sqrt{2ln2}$. Thus, the broadening of our absorption spectrum is determined by the temperature and Rubidium's rest mass;

$$\Delta\nu_{\text{FWHM}} = \sqrt{\frac{8k_BTln2}{mc^2}}\nu_0 \tag{4}$$

B. Doppler-Free Spectroscopy

We seek to resolve our absorption spectrum beyond its Doppler-broadening, in order to do so, we perform what is known as "Saturated" or "Doppler-Free" spectroscopy. We can employ these methods in order to resolve absorption fringes which are very close together.

Carrying out this method involves three beams, the **probe** and **reference** beams along with a high-intensity **saturating** beam. The arrangement of our optical bench containing this set up is described wholly in the following *Experimental Procedure* section.

C. Atomic Transitions

From here we will delve into the quantum mechanics of our experiment, using the following notation to describe the electron configuration in Rubidium: $[(1s^2)(2s^2)(2p^6)(3s^2)(3p^6)(4s^2)(3d^{10})(4p^4)]5s$.

The valence electron occupies the outermost energy level, $n = 5$. Aside from this outlying particle, the *Core Ion* of the atom is spherically symmetric. Although the shell model of atomic structure is inaccurate in many ways, the following graphic shows the intended symmetry;

Thus, it has a total orbital angular momentum number $L_c = 0$, and total spin angular momentum quantum number of $S_c = 0$. So the core ion $Rb+$ has total angular momentum quantum number $J = 0$;

$$|L_c - S_c| \leq J_c \leq |L_c + S_c| \Rightarrow J_c = 0 \tag{5}$$

Since all the aforementioned values are identically zero, the *coupled electronic quantum numbers* all come from our valence electron in whichever (nl) orbital it occupies.

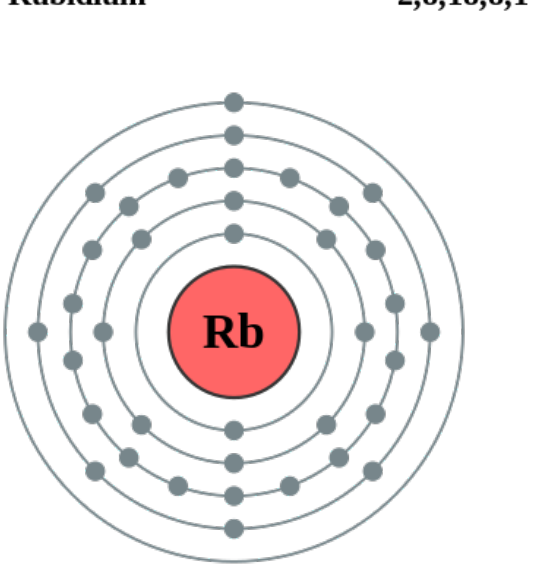

FIG. 2. The nucleus of a Rubidium atom surrounded by five energy levels, where the outermost *Valence* electron surrounds a spherically symmetric core ion.

1. (5s) Ground State

We define "fine-structure" splittings as two states with identical spin and orbital values which can differ in total angular momentum. The $(5s)$ or ψ_500 state has spin $S = 1/2$ but $l = 0$, thus $J = 1/2$ is the only possible value. However, we will see there is some abnormal behavior in our spectral absorption for this state.

This results partially from a phenomenon known as the "Lamb Shift," and also from Hyper-fine splitting (Spin-Spin coupling). The latter's effect is quite noticeable in our other transitions, and it more appropriately explained after the dominating effect on this state.

The Lamb-Shift, which comes from our classical treatment of the electromagnetic field in an otherwise quantized study, is an example of "radiative correction" in Quantum Electrodynamics and can be explained using Feynman's loop diagrams.

The calculation of this effect vastly outreaches the physics of our experiment, but the results are as follows: for $l = 0$,

$$\Delta E_{lamb} = \frac{\alpha^5 mc^2}{4n^3}k(n,0) \tag{6}$$

Here, $k(n,0)$ is a small factor that has very slight variance in regards to n when $l = 0$. ($k(n,0) = 12.7$ when $n = 1$ and $k(n,0) = 13.2$ as $n \Rightarrow \infty$.) [Griffiths, p167/183].

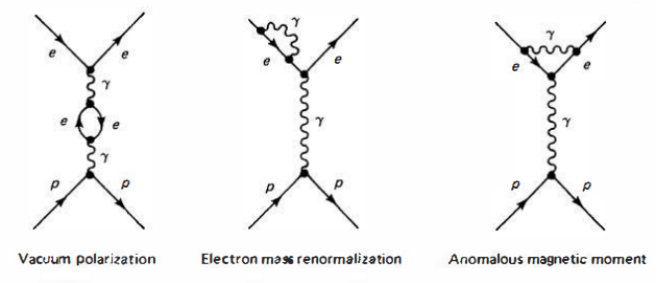

FIG. 3. Some Loop diagrams contributing to the Lamb-Shift

But when $l \neq 0$ there are still more alterations to our spectra, let us examine the splittings of further transitions.

2. *Fine-Structure Splitting*

Now, considering the nonzero orbital momentum of our first excited state $(5p)^2P_{1/2}$, we revisit our earlier equation; $|L-S| \leq J \leq |L+S|$.

We see that $|1-1/2| \leq J \leq |1+1/2| \Rightarrow J = \frac{1}{2}, \frac{3}{2}$. Qualitatively, our electron's probability distribution is no longer spherically symmetric and the dynamics of this moving charge must be considered. Solutions to Schroedinger's equation which describe electron's bound states leave out two non-trivial mechanisms;

1. Relativistic corrections to the Hamiltonian
2. Spin-Orbit coupling (Each verb to be taken lightly)

In the electron's reference frame, a positively charged nucleus "orbits" around it, creating a magnetic field B.

Then, an electron "spinning" with spin S creates a small magnetic field, endowing it with a Dipole moment $\mu_e = -\frac{e}{mc}S$.

The "Spin-Orbit" term is the resulting magnetic energy $-\mu_e \mathbf{B}$. For a state with total angular momentum $j = l \pm \frac{1}{2}$, our resulting energy difference is given by the following equation[5].

$$\Delta E_{fine} = \frac{\alpha^4 mc^2}{4n^4}\left(\frac{3}{2} - \frac{2n}{(j+1/2)}\right) \tag{7}$$

There are names given to certain atomic transitions, in Rubidium, exciting $(5p)^2S_{1/2}$ to the $(5s)^P_{3/2}$ is called the "D_1 line", and $(5p)^2S_{1/2}$ to the $(5s)^P_{3/2}$ state is called the D_2 line. These are of particular importance in practices such as laser cooling.

3. *Hyper-fine Splitting*

Fine-structure splitting is a result of Spin-Orbit interaction, but we mustn't forget the nucleus is a charged particle capable of exhibiting not only "spin" **I** but also possesses an electric quadruple moment, **Q**. In weak magnetic fields, the two quantum numbers I and J couple to give the "grand-total" angular momentum number **F**. As before, we have the restriction;

$$|I-J| \leq F \leq |I+J| \tag{8}$$

To derive the energy spacing of our energy level splittings, we cannot use traditional methods of finding the potential $V(r)$ and substituting into the Schrodinger equation– we observe the spherical symmetry of our Rubidium's core ion and use our Hydrogenic model as an estimate.

A major contributor to this energy-level splitting is the magnetic dipole created by the nucleus, which we express as

$$\hat{M}_n = g_n \mu_n \hat{I} \tag{9}$$

Where g_n is the gyromagnetic ratio of our atom's nucleui (plural because we're using two isotopes of Rubidium).

Our middle term is given in terms of the electron and proton masses; $\mu_n = \frac{e\hbar}{2m_p} = \frac{m_e}{m_p}\mu_B$ where μ_B is the Bohr magneton.

The valence electron has spin $S = \frac{1}{2}$, thus in the lab frame creates a magnetic flux density $\hat{B}_e$.

Interaction between these two systems is given by the Hamiltonian;

$$H_{M1} = -\hat{M}_N \cdot \hat{B}_e \tag{10}$$

For electrons in states $\psi_{n00}(\hat{r})$ (where $l = 0$) we have a spherically symmetric core ion, giving us;

$$\hat{M}_e = -g_s \mu_B s |\psi_{n00}|^2 \tag{11}$$

Where $-g_s\mu_B s$ is the total magnetic moment of our electron.

According to conventional electrostatics, the magnetic flux density inside a sphere with uniform magnetization $\hat{M}$ is

$$B = \frac{2}{3}\mu_0 \hat{M} \tag{12}$$

Before we can substitute M_e into our equation, we assume there is a small sphere of radius δr which encloses the nucleus, and make the approximation

$|\psi_{n00}(\delta r)|^2 \approx |\psi_{n00}(0)|^2$. This gives us

$$B = \frac{-2}{3}\mu_0 g_s \mu_B |\psi_{n00}(0)|^2 s \tag{13}$$

When substituted into equation (eqn) along with (eqn), up to a constant we get;

$$H_{M1}^{l=0} = g_n \mu_n \cdot I \cdot \frac{2}{3}\mu_0 g_s \mu_B |\psi_{n00}(0)|^2 s = \alpha I \cdot s = \alpha I \cdot J \tag{14}$$

The last of those relations stems from $l = 0 \Rightarrow s = J$.

Now, we shift our basis to provide a good description of our system, as neither $I \cdot B$ nor $J \cdot B$ remain constant while precessing about F. We do see, however, that F^2 and m_F are quantum numbers that provide such a basis, and thus we will describe our states as $|\gamma I J F m_F\rangle$, γ serving as any relevant index we left out.
Before moving on, we will find it useful to derive the identity;

$F^2 = F \cdot F = (I + J)(I + J) = I^2 + 2I \cdot J + J^2 \Rightarrow \frac{F^2 - I^2 - J^2}{2} = I \cdot J$

A final note; our state $|\gamma I J F m_F\rangle$ is a simultaneous eigenket of J^2, I^2, and F^2 since they are mutually commuting operators. Thus, in the $l = 0$ case;

$\Delta E_M 1 = \alpha \langle \gamma I J F m_F | I \cdot J | \gamma I J F m_F \rangle$

$= \frac{\alpha}{2}(F(F+1) - I(I+1) - J(J+1)) = \frac{\alpha}{2} C$

Choosing to represent I, J and F as dimensionless quantities gives us our constant of proportionality α dimensions of energy.
In order to derive the $l > 1$ case, perturbation theory and other physics beyond this experiment are required [See Physics of Atoms and Molecules by Brandsen].

$$H_{M1}^{0 \leq l} = \alpha I \cdot J \tag{15}$$

This was merely the magnetic dipole interaction of our Hyper-fine structure Hamiltonian. The Electric Quadrupole interaction is given by

$$H_{E2} = \beta \frac{3(I \cdot J) + \frac{3}{2} I \cdot J - I^2 J^2}{2I(2I-1)(2J-1)} \tag{16}$$

Again, this derivation can be found in [Brandsen].
Finally, we can write the Hamiltonian as a combination of the quadrupole term and the dipole interactions each with their respective constants;

$$\hat{H} = \alpha I \cdot J + \beta \frac{3(I \cdot J) + \frac{3}{2} I \cdot J - I^2 J^2}{2I(2I-1)(2J-1)} \tag{17}$$

The second term vanishes unless I and J are both greater than 1. Plugging the respective quantum numbers into our equation, we find that the change in energy ΔE for the $(5s)^2 S_{1/2}$ state is

$$^{87}Rb \begin{cases} F = 1 & \frac{5\Delta W}{8} = \alpha_{87} \frac{5(I+1/2)}{8} \\ F = 2 & \frac{3\Delta W}{8} = \alpha_{87} \frac{3(I+1/2)}{8} \end{cases}$$

$$^{85}Rb \begin{cases} F = 2 & \frac{7\Delta W}{12} = \alpha_{87} \frac{7(I+1/2)}{12} \\ F = 3 & \frac{5\Delta W}{12} = \alpha_{87} \frac{5(I+1/2)}{12} \end{cases}$$

From these four equations we get

$$\begin{cases} \Delta W_{87} = 2a_{87} \\ \Delta W_{85} = 3a_{85} \end{cases}$$

Graphically, all these transitions and their fine/hyper-fine splittings can be seen here;

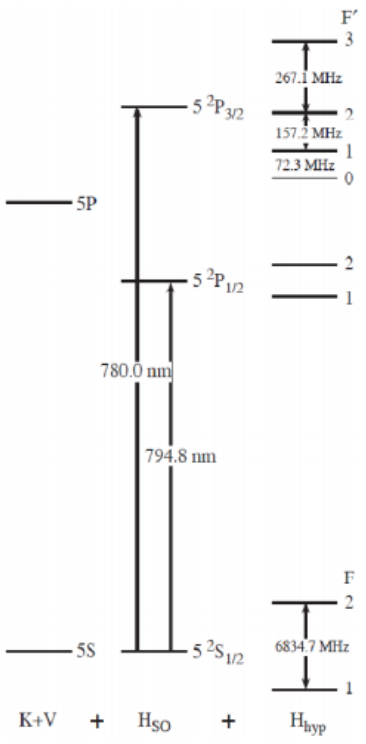

FIG. 4. Wavelengths λ corresponding to Rubidium's excitation Energies $E_\gamma = hc/\lambda$

II. EXPERIMENT

A. Apparatus

In this experiment, we use the optical bench pictured in Figure 3 below. A diode laser with a variable current is used to create a beam that is targeted at plexiglass at an angle to the incident light. This glass splits the beam, such that some of it continues on straight and some is diverted orthogonal to incoming radiation. The diverted beam then travels through the Rb cell, and on to a beam splitter, behind which are two photodiodes. The beam that was not diverted hits a mirror that directs it at an angle to meet the other beam at the photodiodes. Note that this second beam is blocked by a removable flap, and is only used when we examine the hyper-fine splittings associated with the Doppler shift between the two beams (which have traveled different distances at the photodiodes). After the beam splitter, the beam travels to a Febry-Perot Interferometer (not pictured), which from which we take our data on the spectroscopy of the Rb in question.

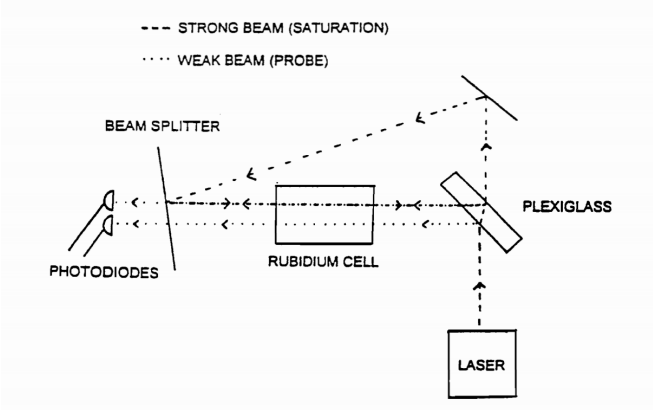

FIG. 5. This assembly was created to be able to take data. Note that not pictured here is a Fabry-Perot Interferometer, which received light from the beam splitter and is located close to the diode laser.

The observations of the Fabry-Perot are displayed on an oscilloscope, while another oscilloscope shows the amplitude and oscillations of the triangle-wave employed to the laser. We are able to control the frequency and amplitude of the current supplied to the laser, as well as the current itself, which frequently oscillates around whatever value that we choose.

B. Procedure

During measurement, we used the following values for the specifications described above: frequency - 78.80 Hz, amplitude - 38.00 V, current - $110 \pm 5A$. These values allowed us to observe the two peaks resulting from the Fabry-Perot measurements, in addition we were able to see the absorption spectrum of the two isotopes of Rb examined. Using the oscilloscope to zoom and focus the image (both channels) we took data using a flash drive of one whole triangle wave and the resulting interference patterns on the Fabry-Perot (Fig. 4), as well as the absorption spectrum of the Rb isotopes (Fig. 5). We found the spacing between the Fabry-Perot peaks, in which the absorption spectrum would be observed. Additionally, we found the distance between the two larger peaks (corresponding to ^{87}Rb), and the two smaller peaks (^{85}Rb). We also found the FWHM of the peaks in the absorption spectrum. The results of this analysis are shown in the Data section of this report below.

Zooming in on each individual peak, we set the oscilloscope so that we could take a close-up picture of each curve. We also took data using this close-up view on the hyperfine structures of each Gaussian-like curve (removing the flap on the mirror behind the plexiglass such that the weak beam could factor into the results). Saving this data, we proceeded with our analysis.

III. ANALYSIS

A. Non-Saturated Spectrum

In order to appreciate the improved resolution of the Doppler-Free method, let us examine the unsaturated absorption spectrum. To take accurate measurements, we need to know our scale on the oscilloscope, which can be found by finding the spacing between resonances in our Fabry-Perot data. In order to do this, we varied the range of out AC signal which served as the power source for our diode laser, thus controlling the output frequency/ wavelength The two are of course related since the speed of light is constant; $c = \lambda\nu$.
Note that in Figure 4, the sharp peaks correspond to when the cavity's separation distance d is a half-integer multiple of the laser beam's wavelength λ;

$$d = \frac{n\lambda}{2},\ n \in \mathbb{Z} \tag{18}$$

This relation will allow us to discern our the ratio between our timescale and the variance in frequency, ν. The AC signal which powers our diode laser is a Triangle Wave, and thus the signal's amplitude changes linearly in time, which causes a linear change in our beams output frequency. The **Free Spectral Range** of our Fabry-Perot, or the range of output frequency allowed by the space of the cavity, d, is

$$\Delta\nu = \frac{c}{2d} = \frac{299792458[m/s]}{2 \times 0.015[m]} \approx 9.99308 * 10^9 \tag{19}$$

Thus, after finding the distance between two peaks each at t_1 and t_2, we can convert our future measurements of time difference to the corresponding change in frequency by multiplying by $\frac{c}{2d\Delta t}$.

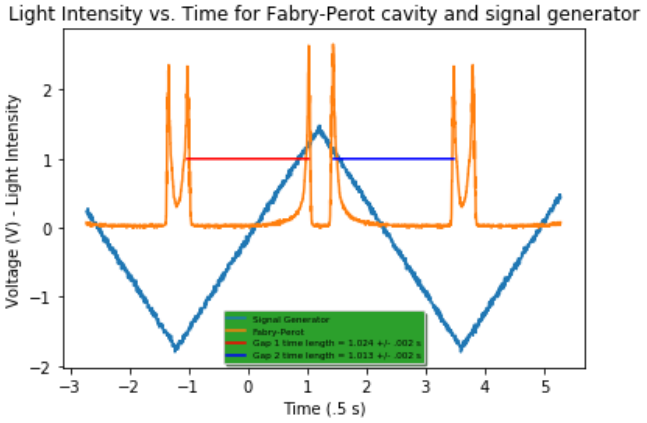

FIG. 6. Light Intensity as a function of time for our Fabry-Perot cavity, plotted alongside the AC signal powering our Diode laser. The units of time are half seconds

Now that our measurements can be given physical significance using our conversion factor, we move onward analyzing our data. Our absorption spectrum without saturation can be seen in the following figure;

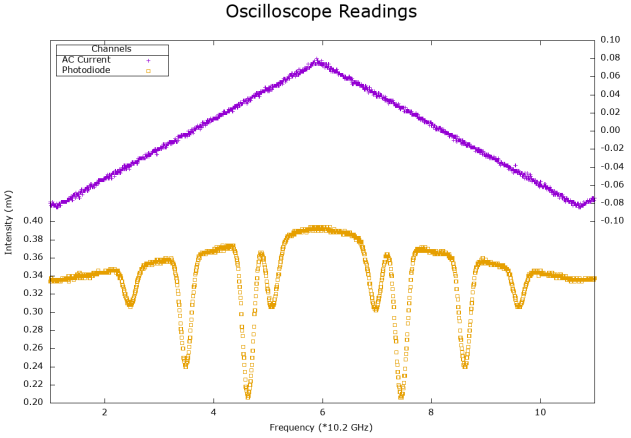

FIG. 7. Absorption spectrum of ^{85}Rb and ^{87}Rb at room temperature.

Since our particles' random velocity follows a Gaussian distribution, we derived earlier that the width of these curves should follow the relation;

$$\Delta\nu_{\text{FWHM}} = \sqrt{\frac{8k_B T ln2}{mc^2}}\nu_0 \tag{20}$$

We can use software to fit Gaussian curves to our data in order to most accurately find the full width, half max. We did so by assuming a functions of the form;

$$f_i(x) = a_i exp(-\frac{(x-\mu_i)^2}{2\sigma_i^2}) + c_i \tag{21}$$

Once this is done and our fitted curves strongly correlate with our data, we can analyze the σ and μ parameters, and compare our results to the theoretical band-widths, where $\Delta\nu_{\text{FWHM}} = \sigma$ and $\mu = \nu_0$.

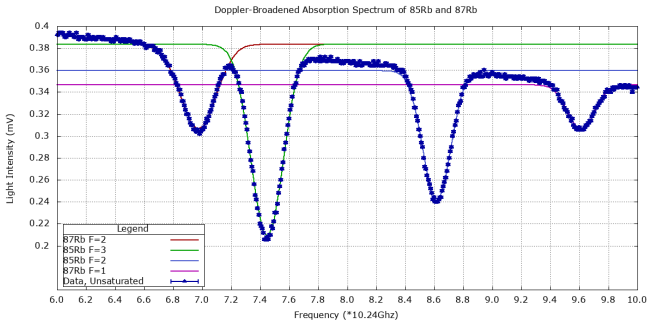

FIG. 8. Unsaturated absorption spectrum, with associated Gaussian Fits. The error bars from the original data stem from the uncertainty in the oscilloscope readings, with uncertainties of .001 along each axis.

To demonstrate the correlation between the predicted values and our data, we can plot the fitted curves separately. By taking the amplitudes to be positive and setting the added constants equal to zero, we can clarify the results without any added inaccuracy.

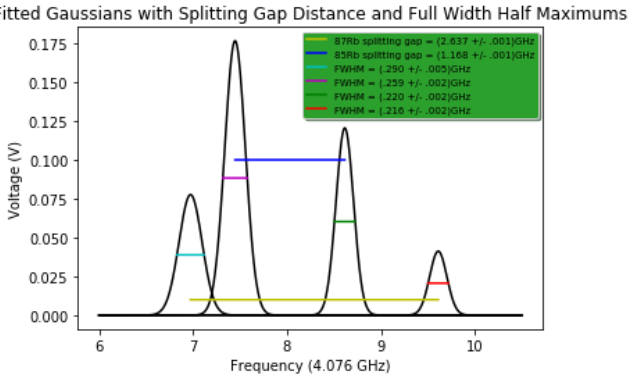

FIG. 9. Plotted Gaussian curves without data. The full-width, half max values for each curve are shown along with the peak distances.

Now, although we have a well defined measure for **relative frequency** i.e. the change in frequency per second

of our axis, this does not tell us the specific frequencies v_i occurring at a given time. But by taking the slope, we may find some relation between them. The following table gives both $\Delta\nu_{\text{FWHM}}$ values, calculated by equation (4) and by taking $2\sqrt{2ln2}\sigma$

Gaussian Width

Width	Experimental (s)	Theoretical (s)
$\Delta\nu_{\text{FWHM1}}$	$(2.90 \pm .005) \times 10^{-1}$	$(2.062 \pm 0.03) \times 10^{-5}$
$\Delta\nu_{\text{FWHM2}}$	$(2.59 \pm .002) \times 10^{-1}$	$(2.202 \pm 0.03) \times 10^{-5}$
$\Delta\nu_{\text{FWHM3}}$	$(2.20 \pm .002) \times 10^{-1}$	$(2.548 \pm 0.03) \times 10^{-5}$
$\Delta\nu_{\text{FWHM4}}$	$(2.16 \pm .002) \times 10^{-1}$	$(2.842 \pm 0.03) \times 10^{-5}$

We found that the two slopes are as follows;

$$\frac{\partial\Delta\nu_{\text{FWHM}}}{\partial t} = \begin{cases} (2.957 \pm 0.030) \times 10^{-6} & \text{Theoretical} \\ (-2.932 \pm 0.525) \times 10^{-2} & \text{Experimental} \end{cases}$$

In order to give relative distances between peaks, we shall invoke our conversion factor, Ω, given by the free spectral range divided by the original difference in time,

$$\Delta\nu \approx 9.99308 \times 10^9 \Rightarrow \Omega = \frac{9.99308}{1.024} \times 10^9 \approx 9.75887 * 10^9 \tag{22}$$

The following table holds our measured values for the separation between absorption frequencies, first in unconverted (s) form and then again in Hz.

Distance between Absorption Frequencies

^{87}Rb Peak Distance	$(1.319 \pm .001)s$	$1.286 \times 10^10 Hz$
^{85}Rb Peak Distance	$(0.584 \pm .001)s$	5.699×10^9

In a perfect world, we would have obtained frequencies equal to our expected values, namely;

$$\Delta\nu = \begin{cases} 6834.683(2)MHz & ^{87}Rb \\ 3035.735(2)MHz & ^{85}Rb \end{cases}$$

But fret no more, because we can examine the *ratio* between these measurements;

$$\frac{6.834(2)}{3.035(2)} \approx 2.2517 \pm 0.002 \tag{23}$$

Now, comparing this to the ratio of our acquired values;

$$\frac{1.319}{0.584} \approx 2.2586 \pm 0.001 \tag{24}$$

Evidently, the ratio of our answers is not far off from the expected values' ratio.
Now that we have treated our unsaturated data, we can move on to our Doppler-Free spectrum.

B. Doppler Free Spectroscopy

Recall that hyperfine splitting is a result of the *Grand* total Angular Momentum quantum number **F** taking on values between $|\mathbf{I} - \mathbf{J}|$ and $|\mathbf{I} + \mathbf{J}|$, where **I** is the Spin quantum number and **J** is the total angular momentum quantum number.

Visually, the difference is clear between this data and the previous examples. First, the D_2 line for ^{85}Rb;

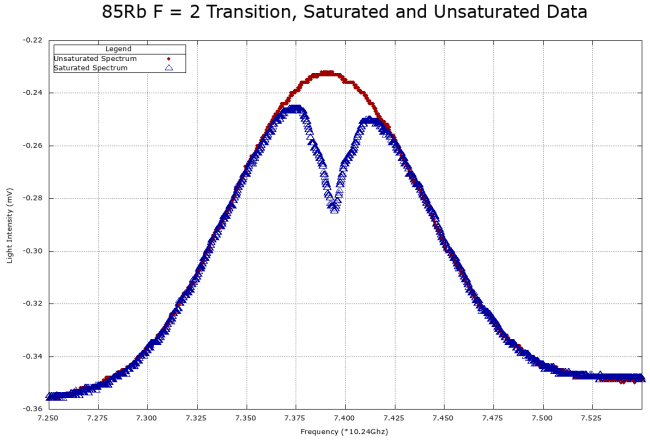

FIG. 10. The saturated and unsaturated data corresponding to the ^{85}Rb F=2 Hyper-fine state

This saturated spectrum has a number of telltale features. Recall the theory we developed previously regarding the Lamb-Shift, where a quantum treatment of electromagnetism gives correction to the classically derived values for absorption frequency. Since Quantum Electrodynamics is well beyond the scope of undergraduate physics, let us focus instead on the other pertinent phenomenon, crossover resonances. Consider two transition frequencies ν_1 and ν_2, each obscured by the broadening of our spectrum. We find that another resonance in between them appears in our data, but it is not a true representation of a potential atomic transition. The following graphic should lend clarity to this concept[14].

As shown in the figure, the "Crossover resonances" occur between two frequencies at $\frac{\nu_1+\nu_2}{2}$, they not only resemble actual transition frequencies but are extremely

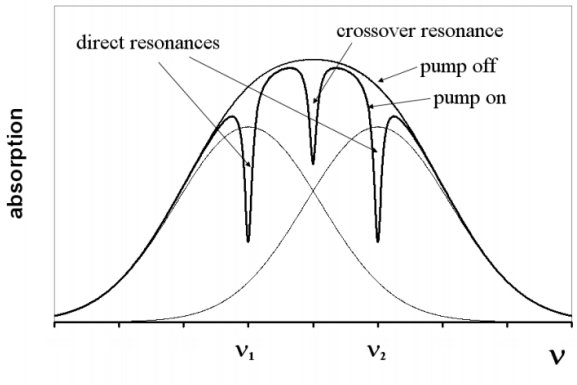

FIG. 11. A graphic display of how crossover resonances arise from closely paired transition frequencies

pronounced relative to their physically significant parent resonances.

We see this may not be the best case study for hyper-fine transitions. Instead, we have prepared our data from ^{87}Rb , D_2 state in the most readily analyzable fashion,;

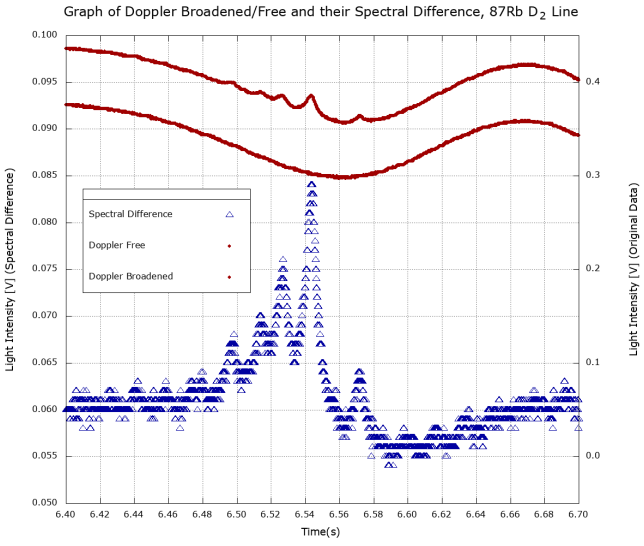

Since the resolution is quite low relative to the size of our hyper-fine splittings, there is quite a bit of uncertainty in some of our measurements. In others, the grouping of data point around each maxima was fairly tight and their respective uncertainties are not as bad. Nevertheless, the following table lists all identifiable energies.

$Time(s)$	$t_0 \times \Omega(GHz)$	$\Delta\nu(MHz)$
6.49809 ± 0.00010	6.34140 ± 0.0001	-44.46 ± 0.10
6.51359 ± 0.00035	6.35652 ± 0.00035	-29.33 ± 0.35
6.52695 ± 0.00005	6.36956 ± 0.00005	-16.29 ± 0.05
6.54365 ± 0.00035	6.38586 ± 0.00035	0 ± 0.35
6.57175 ± 0.00085	6.41328 ± 0.00085	27.42 ± 0.85

The third column is the *difference* in frequency relative to the highest, central peak.

It would be redundant to tabulate the theoretical values, as they are given in our diagram on page 4 and can be found in many other places.

This concludes the analysis portion of this experiment. Allow my partner to lead us out.

IV. CONCLUDING REMARKS

There were many possible sources of systemic error in this experiment, including but not limited to variances in temperature within the room, small vibrations on the apparatus board, and variances in the air. These sources are negligible for the purposes of this experiment and can be ignored within our results.
Statistical error played more of a role within our measurements, as there were certain limitations to the observing power of the oscilloscope, as well as randomized oscillations of the current. Additionally, as we calculated our values we assumed that our Gaussian fittings were good to a reasonable estimate of the data we took, given the chi^2 analysis of the fitting software we used (Gnuplot). Thus, our errors propagated throughout the calculation portion of the Unsaturated absorption spectroscopy part of this experiment. That being said, our uncertainties were still very minute compared to the values we ended up with (δ around $\frac{1}{100}$ of the magnitude of our measurements, and thus even if the theoretical values of FWHM were outside the δ range, they are still reasonably close to support the theory discussed in the Introduction. Thus, this portion of our lab was statistically significant enough to support the theory of the Unsaturated Absorption Spectroscopy of Rubidium Isotopes.

REFERENCES

[1] American Physical Society, "December 1958: Invention of the Laser," This Month in Physics History, vol. 12, no. 11, December 2003.

[2] American Physical Society, "Einstein Predicts Stimulated Emission," This Month in Physics History, vol. 14, no. 8, August/September 2005.

[3] A. Einstein, "The Quantum Theory of Radiation," Physikalische Zeitschrift, March, 1917.

[4] MIT Department of Physics, "Doppler-Free Spectroscopy," Nov. 29, 2012.

[5] T. Rieger and T. Volz, "Doppler-Free Saturation Spectroscopy," Max-Plank-Institut fur Quantenoptik.

[6] Wolfram Research, "Hyperfine Splitting," scienceworld.wolfram.com.

[7] University of Maryland, "Magnetic Dipole Transition in Rubidium87," terpconnect.umd.edu.

[8] L. P. Maguire, R. M. W. van Bijnen, E. Mese, and R. E. Scholten, "Theoretical calculation of saturated absorption spectra for multi-level atoms," IOP Science Journal of Physics B: Atomic, Molecular and Optical Physics, vol. 39, no. 12, May 24, 2006.

[9] D. Griffiths, *Introduction to Elementary Particles* (Academic, Oregon, 2008).

[10] S. S. San, S. Bennetts, J. E. Debs, C. C. N. Kuhn, G. D. McDonald, P. A. Altin, J. D. Close, and N. P. Robins, "11 W narrow linewidth laser source at 780nm for laser cooling and manipulation of Rubidium," The Optical Society, Optics Express, vol. 20, issue 9, pp.8915-8919, 2012.

[11] Wolfram Research, "Lamb Shift," scienceworld.wolfram.com.

[12] Lab manual, "Measuring the Hyperfine Levels of Rubidium Using Saturated Absorption Spectroscopy," Georgia Technical Institute Advanced Lab.

[13] Lecture Notes, "Atomic Spectra," Menning, K. Univ. Wisconsin at Stevens Point. [14] Lab Manual, "Saturated Absorption Spectroscopy," Univ. of Florida, Advanced Physics Laboratory.